Electrical detection of excitonic states by time-resolved conductance measurements

C. Ebler,[1,*] P. A. Labud,[1] A. K. Rai,[1] D. Reuter,[2] A. D. Wieck,[1] and A. Ludwig[1]
[1]*Chair of Applied Solid State Physics, Ruhr-University Bochum, Universitätsstraße 150, D-44780 Bochum, Germany*
[2]*Department Physics, University Paderborn, Warburger Straße 100, D-33098 Paderborn, Germany*

(Received 19 July 2019; revised manuscript received 3 January 2020; accepted 3 March 2020; published 18 March 2020)

We present time-resolved conductance measurements and charge spectra for the conduction-band states of InAs quantum dots after creating metastable holes by illumination. We demonstrate an electrical way of measuring the conduction-band energy offset and inverse tunnel rates of electrons from a two-dimensional electron gas into neutral (X^0), single positively (X^{1+}), and double positively (X^{2+}) charged exciton states. The experiment also gives information about the metastable hole storage time and discharge dynamics.

DOI: 10.1103/PhysRevB.101.125303

I. INTRODUCTION

Self-assembled quantum dots are nanoscale objects which are suitable for classical optical data communications [1], as well as potential candidates for novel technologies, such as quantum dot (QD) flash memories [2]. By using QDs in proper charge tuneable semiconductor heterostructures and varying the gate voltage, the creation of charged and neutral excitons was demonstrated by photoluminescence measurements [3]. Using resonant excitation schemes in resonance fluorescence experiments [4], purely transform-limited single-photon emission [5] brings quantum cryptography and optical quantum computing in a realistic scenario, applying these high-quality QDs. Recently, the influence of continuous light on special *n*-type QD-capacitance-voltage-spectroscopy structures was investigated, where charged excitons up to X^{4+} were electrically detected [6]. Marquardt *et al.* [7] presented an electrical method which allows for equilibrium and nonequilibrium [8] QD electron state spectroscopy by using a two-dimensional electron gas (2DEG) (Fig. 1) as a detector for the electron charge in the QDs and recording the tunneling dynamics from the 2DEG into the QDs. We will refer to this method as transconductance spectroscopy $G(V, t)$, as the conductance of the 2DEG is measured as a function of applied bias and time.

In this paper, we present an extension of the $G(V, t)$ in which we integrate a light pulse in the voltage sequence (Fig. 2) to create nonequilibrium holes in the QDs. We confirm the results of Labud *et al.* [6] by electrically detecting excitons in QDs and measure the tunneling dynamics of electrons in exciton states with time delays between the hole generation and readout of up to 4 s.

II. EXPERIMENT

A. Sample structure

We study the temporal evolution of the conductance of a 2DEG that is coupled to a layer of self-assembled QDs. The relevant layer sequence starts with 300 nm undoped $Al_{0.34}Ga_{0.66}As$, followed by a Si delta doping (i.e., 10 min of Si deposition), covered by 16 nm undoped $Al_{0.34}Ga_{0.66}As$ which serves as a spacer. Afterward, 15 nm GaAs is deposited in which the 2DEG is formed. 10 nm $Al_{0.34}Ga_{0.66}As$ and 5 nm GaAs form a tunnel barrier to the following QD layer. For the QD growth, the substrate temperature is reduced from 600 to 525 °C and the As flux was approximately halved (from 13 to 6.8×10^{-6} Torr and a single layer of InAs QDs was grown by depositing approximately 2 monolayers InAs, followed by 8 nm GaAs grown at 500 °C. Raising the temperature back to 600 °C, the structure is finalized by 35 periods of a 3 nm AlAs/1 nm GaAs short period superlattice (SPS) and a cap layer of 5 nm GaAs. The QD density is in the order of 10^{10} and the 2DEG charge-carrier density taken from Hall measurements is constituted to $n_e = -7.6 \times 10^{11}$ cm^{-2}.

A specialty of this structure is that the GaAs layer, which caps the InAs islands, has to be thin in order to avoid unwanted charge accumulation from illumination at the interface to the short period superlattice [6,9]. From this heterostructure a field-effect transistor structure is fabricated by etching a mesa channel with two alloyed NiGeAu ohmic contacts (source and drain) and a 20-nm-thick Au layer as a Schottky gate, semitransparent to light.

B. Experimental setup and measurement procedure

All experiments are performed in a liquid-helium vessel with gaseous He thermal contact at 4.2 K. For capacitance-voltage $C(V)$ spectroscopy measurements [6], we use a lock-in amplifier where a DC+AC voltage ($V_{AC} = 10$ mV$_{rms}$, $f = 37$ Hz) is applied to the Schottky gate and the resulting AC charge/discharge current is lock-in recorded at the source contact. While the in-phase current is negligible, an out-of-phase ($-90°$) current typically of 150 pA can be converted to a capacitance value ($C \approx 60$ pF).

In the $G(V, t)$ measurements, the source contact is grounded and the drain contact is biased with 40 mV by a low noise transimpedance amplifier, converting the current through the 2DEG into a voltage. This voltage is recorded in

*carsten.ebler@rub.de

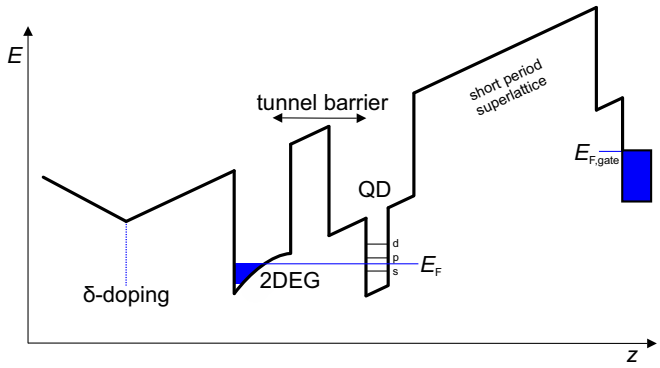

FIG. 1. Conduction-band structure sketch of the sample. The blue line indicates the Fermi energy E_F. The tunnel barrier between the 2DEG channel and the QDs consists of 10 nm $Al_{0.34}Ga_{0.66}As$ and 5 nm GaAs. The InAs QD confinement includes a sketch of the *s*, *p*, and *d* shells.

a time-resolved manner by an oscilloscope. The gate is biased by a programmable arbitrary wave-form generator (AWG), following the pulse sequence depicted in Fig. 2.

V_G is the DC gate voltage that is applied to bring the different states in the QD in resonance with the Fermi level of the 2DEG. Partial charging is induced by an additional voltage pulse of the level $V_C = 20$ mV to the gate. Up to here, the sequence is identical to the experiment described by Marquardt *et al.* [7]. In addition to that, a light-emitting diode ($\lambda_{4.2\,K} \sim 920$ nm) is placed in front of the gate. In each measurement cycle, a synchronized light pulse is sent to the sample by applying a current pulse from a programmable current source with a timing advance of Δt (Fig. 2). The LED current is 5 mA with a pulse duration of 200 ms. A reset pulse with a much higher voltage than V_C is necessary in our experiment to erase (remove) all residual holes after one measurement cycle. Since the reset pulse is just a technical necessity, $t = 0$ for the absolute time scale is set to the beginning of the light pulse. All measurements are repeatedly co-added for each V_G to average the signal and thus suppress the noise (typically 200 averages).

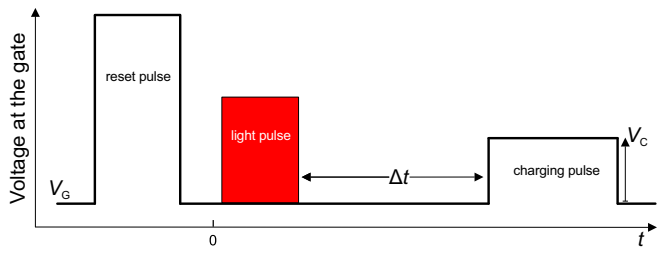

FIG. 2. Light and gate charging pulse sequence. At the beginning of the sequence, a reset pulse with a high voltage is sent to the device to remove the remaining holes in the QDs in order to restore the same initial conditions for the averaging. While the gate voltage V_G is applied, a light pulse of adjustable duration and intensity excites electron-hole pairs in the sample. After a delay time Δt, the voltage at the gate is increased with a charging pulse V_C. Since the reset pulse is just a technical necessity, $t = 0$ for the absolute time scale is set to the beginning of the light pulse.

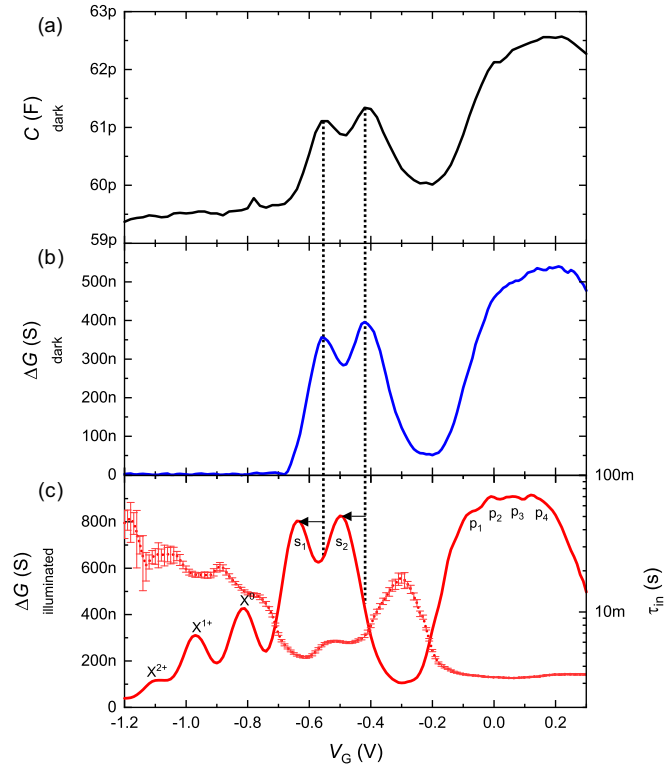

FIG. 3. (a) $C(V)$ measurement (black curve) and (b) $\Delta G(V, t)$ measurement (blue curve) without illumination. The two *s*-state charging peaks are clearly visible in both spectra. The four *p* states cannot be distinguished without further analysis due to ensemble broadening. (c) $\Delta G(V, t)$ measurement (red curve) with a light pulse in the gate voltage sequence (Fig. 2). Three clear additional charging peaks can be detected which correspond to the charging of excitons X^0, X^{1+}, and X^{2+}. For the illuminated spectra, all pure electron states are shifted to a lower gate voltage due to the higher Fermi level in the 2DEG from the strong illumination and charging of *DX* centers before these measurements. τ_{in} is determined from exponential fits on the charging transients (Fig. 5) and represents the gate voltage dependent tunnel coupling.

III. MEASUREMENTS AND INTERPRETATIONS

In addition to the $G(V, t)$ measurement results with the extension of a light pulse, we compare $C(V)$ and $G(V, t)$ measurements without illumination. From $C(V)$ measurements [Fig. 3(a)] charging of the 2DEG at $V_G > -1.2$ V and single-electron charging in the electronic states become visible by two separated and one broad peak in the spectrum. The two features at -0.56 and -0.42 V correspond to electron charging in the *s* shell. The twofold spin degeneracy is lifted by Coulomb interaction [10]. The broad peak in the gate voltage range of -0.1–0.3 V consists of four further charging peaks corresponding to the *p* shell. The expected fourfold spin and angular momentum degeneracy is lifted by Coulomb and exchange interaction as well as elongation of the QDs [10–12].

In principal the same result is obtained for the $G(V, t)$ measurements [Figs. 3(b) and 3(c)]. The signal ΔG in the $G(V, t)$ measurements is the difference in conductance of the 2DEG directly after applying the charging pulse V_C and

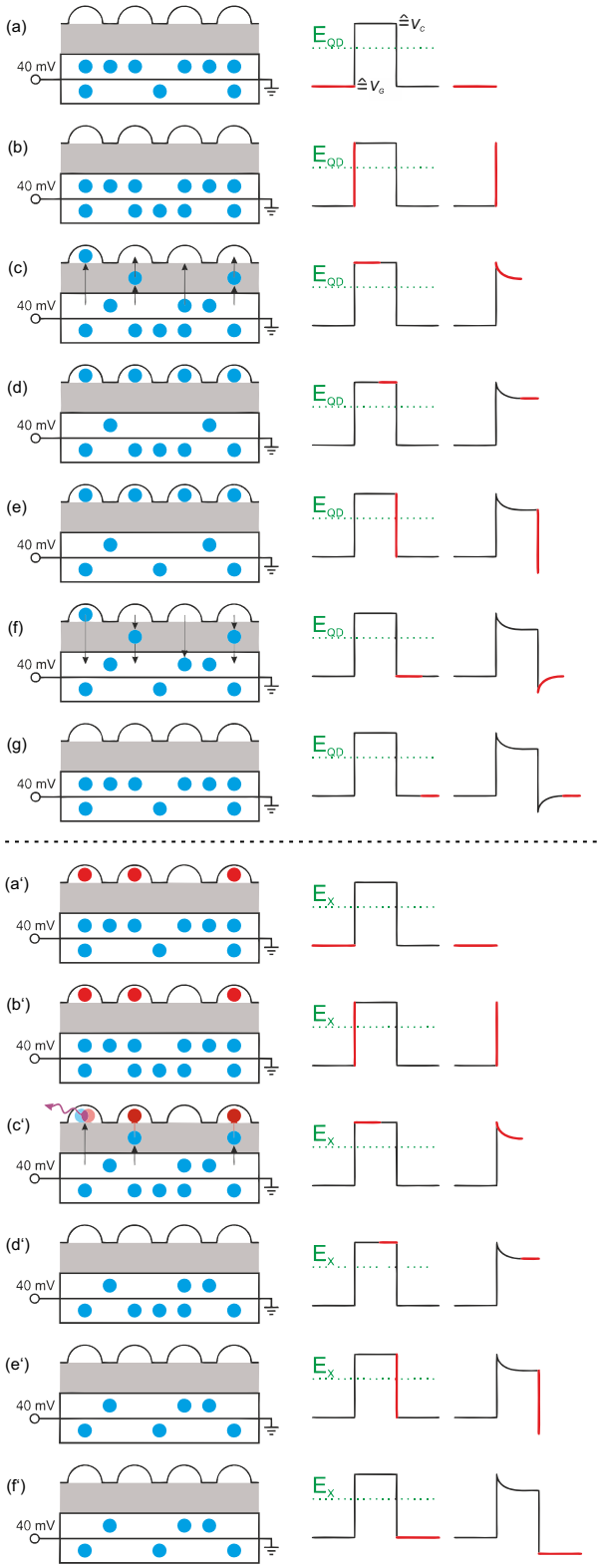

FIG. 4. The sequential voltage of the charging pulse applied to the gate (according to the sequence in Fig. 2) and the conductance measured in the channel for the $G(V,t)$ measurements. The corresponding situation is sketched with electrons (blue balls) in the 2DEG channel and electrons as well as holes (red balls) in the QDs. Electron charging of the QDs (c),(d) and discharging (f),(g) without additional illumination (top) and in correspondence with annihilation of illumination induced hole states (c′) (bottom).

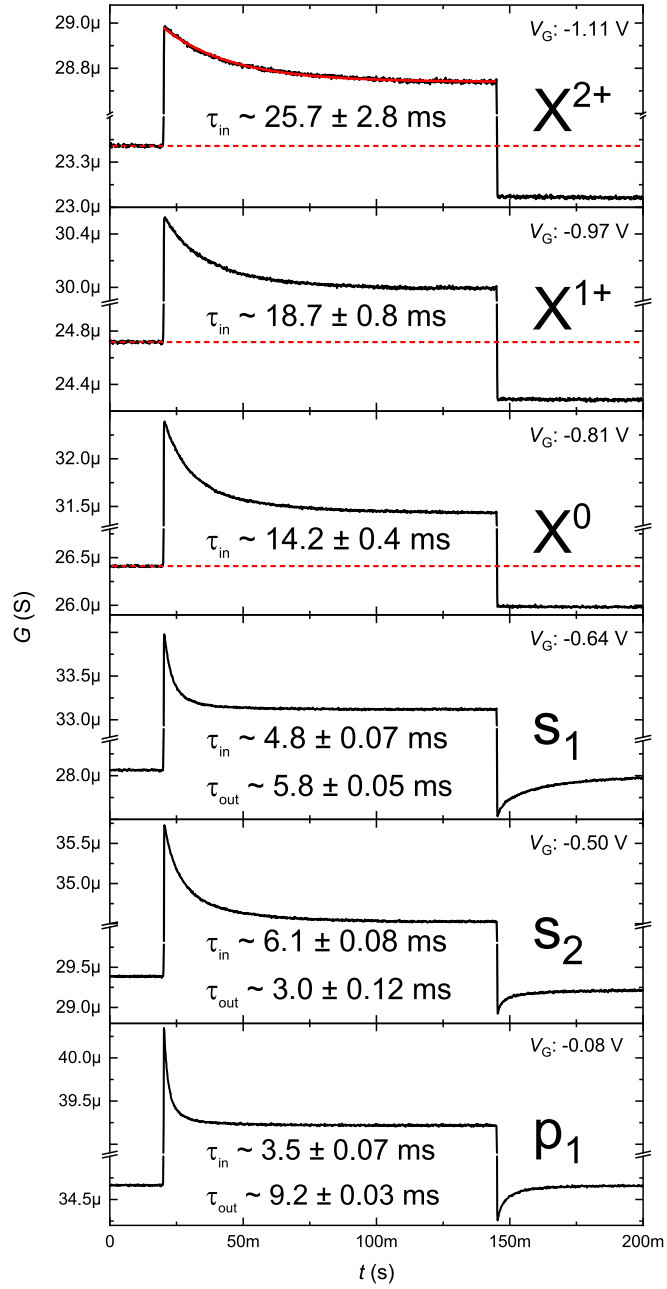

FIG. 5. Channel current response $G(V,t)$ to the charging pulse in Fig. 2 for gate voltages V_G at the $s_{1,2}$, p_1 and excitonic peaks X^0, X^{1+}, X^{2+}. The gate voltage sequence contains a light pulse (duration 200 ms, LED current 5 mA, $\Delta t = 0.5$ s). Time constants τ_{in} and for the s and p charging states and also τ_{out} are determined from exponential fitting functions (red line at X^{2+} as an example) at the transients. Since the tunneling electrons annihilate with the holes inside the QDs for the excitonic states, a reverse tunneling process after the charging pulse cannot be observed but a lower conductance indicated by red dashed lines.

a time delay of 100 ms (see transients in Fig. 5). For the illuminated $G(V,t)$ measurements, we first saturated the DX centers [13,14] in the modulation delta-doped layer by long-time illumination (10 min at 5 mA LED current) before the following $G(V,t)$ spectroscopy measurements. In Fig. 3(c), the $G(V,t)$ measurement under illumination is shown: the

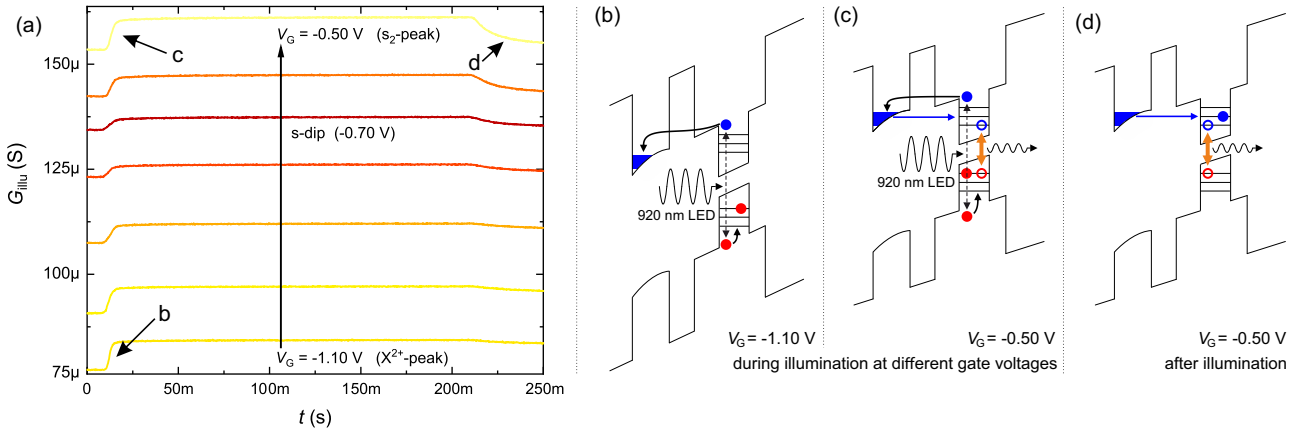

FIG. 6. (a) Conductance response G_{illu} during the illumination with increasing gate voltage. Δ200-ms light pulse starts at 0 ms. The three sketches (b)–(d) depict the conductance and valence band around the QD and 2DEG for $V_G = -1.10$ V and -0.50 V to explain the electron tunneling as well as the electron-hole excitation and recombination responsible for the corresponding change in conductance in (a). The blue arrow in each sketch represents the tunnel coupling between 2DEG and QDs while the black dashed line corresponds to light-induced electron-hole creation. The orange arrow indicates fast typically radiative electron-hole annihilation processes.

difference in conductance ΔG versus the applied gate voltage as well as the according charging time constant τ_{in} calculated with exponential fits on the pulse transient of V_G. The s and p peaks are slightly shifted to a lower gate voltage, compared to the nonilluminated spectra due to saturation of the DX centers and thus increased Fermi energy in the 2DEG by the mentioned preillumination. Apart from that, they stay qualitatively unaffected and three additional peaks appear at $V_G = -0.81$ V (X^0), -0.97 V (X^{1+}), and -1.11 V (X^{2+}).

A simple lever arm approach can be used to transform the gate voltage into energy values for the Coulomb interaction of the states (detailed explanation in [12,15]). The energy separation for the light-induced exciton peaks (e.g., $\Delta E_{s_1 X^0}$) compared to the level splitting of the s_1 and s_2 peaks $\Delta E_{s_2 s_1}$ are

$$\Delta E_{s_2 s_1} = 21.0 \text{ meV}, \quad (1)$$

$$\Delta E_{s_1 X^0} = 28.5 \text{ meV}, \quad (2)$$

$$\Delta E_{X^0 X^{1+}} = 25.7 \text{ meV}, \quad (3)$$

$$\Delta E_{X^{1+} X^{2+}} = 23.3 \text{ meV} \quad (4)$$

with an uncertainty of ±1 meV due to experimental uncertainties and imperfect knowledge of the lever pivot point. The measurement results and the energy values are in relatively good agreement with the values obtained by Labud *et al.* [6].

Up to now, the difference in the channel conductance ΔG has been discussed. This part will give a detailed explantation for the additional graph τ_{in} shown in Fig. 3(c). Therefore the sketches in Fig. 4 show the process of electron charging in empty and hole-filled states and according to that in Fig. 5 the measured temporal evolution of the channel conductance as a response to the charging pulse V_C for different gate biases. As the gate is pulsed to V_C, the conductance rises abruptly (on a sub μs time scale) due to the charging of the 2DEG. When charge states are in resonance with the increased Fermi energy, electron tunneling in the QDs takes place and reduces the channel conductance with an exponential decay on a millisecond time scale. The behavior of τ_{in} was taken from these transients (red fitting function as an example on the X^{2+} transient) and represents the tunnel coupling mainly depending on charge state resonances (X^0, s_1, p_1, etc.) and spin degeneracy features. Since V_C is at 20 mV, we only observe resonant state charging. The more reverse bias, the longer the charging time for the different states due to an increased tunnel barrier height. The exception of s_2 (6.1 ± 0.08 ms) compared to s_1 (4.8 ± 0.07 ms) originates from the spin degeneracy and thus reduced tunneling probability (s_1 spin degeneracy of two and s_2 spin degeneracy of one as one electron is already in the QD for tunneling into s_2) [10]. Pulsing the voltage back to V_G—for the pure electron states s_1, s_2, etc.—a fast discharging of the 2DEG and a slower discharging of the QDs can be seen. The discharging time of s_1 (5.8 ± 0.05 ms) has to be slower than for s_2 (3.0 ± 0.12 ms) as the out tunneling degeneracy is now 1 for s_1 (only one electron in s_1) and 2 for s_2 [10]. Electron tunneling into excitonic states happens on comparable time scales, where the X^0 state time constant (14.2 ± 0.4 ms) is approximately three times the s_1 charging time due to a larger tunnel barrier. Please note that the tunneling happens in the same state as for s_1 [6], but the Coulomb potential of the additional hole changes the energy state and also the potential barrier shape. This continues for X^{1+} (18.7 ± 0.8 ms) and X^{2+} (25.7 ± 2.8 ms). In contrary to the pure electron states [Figs. 4(d) and 4(e)], an electron out tunneling cannot be observed for the excitonic states, since the electron hole recombination leaves the QD in a state that is one elementary charge more negative than before. As a result, the conductance is smaller than before the V_C pulse until a new hole is generated by another light pulse [red dashed line in Figs. 5(a)–5(c)].

We now want to have a deeper look at what actually happens during and after the illumination pulse.

For a full investigation of the light-induced hole creation process and the storage conditions, we want to begin with a detailed look at the 2DEG behavior during the illumination.

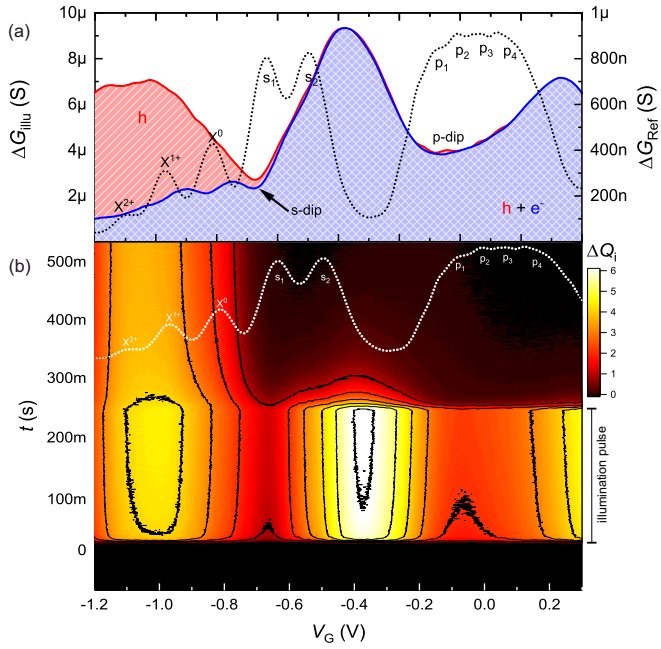

FIG. 7. (a) Conductance difference ΔG_{illu} caused by the illumination. For the red curve the conductance was picked during the pulse at $t = 100$ ms and before at $t = 0$ ms and for the blue curve during the pulse at $t = 100$ ms and after it ended at $t = 300$ ms. All times t originate from the time scale of the sequence shown in Fig. 2. (b) Time-resolved differential evolution of the conductance over the period of the illumination sequence. The resulting $\Delta G(t)$ is transformed into an average amount of light-induced charges ΔQ_{i} per QD (see Fig. 9 in the Appendix). The output represents the time-dependent light induced nonequilibrium of the QDs for all t up to 650 ms. The illumination is active in between $t = 0$ ms and $t = 200$ ms as indicated on the right border. The dotted line ΔG_{ref} in both plots shows the illuminated equilibrium spectra and serves as a reference for charge state resonances.

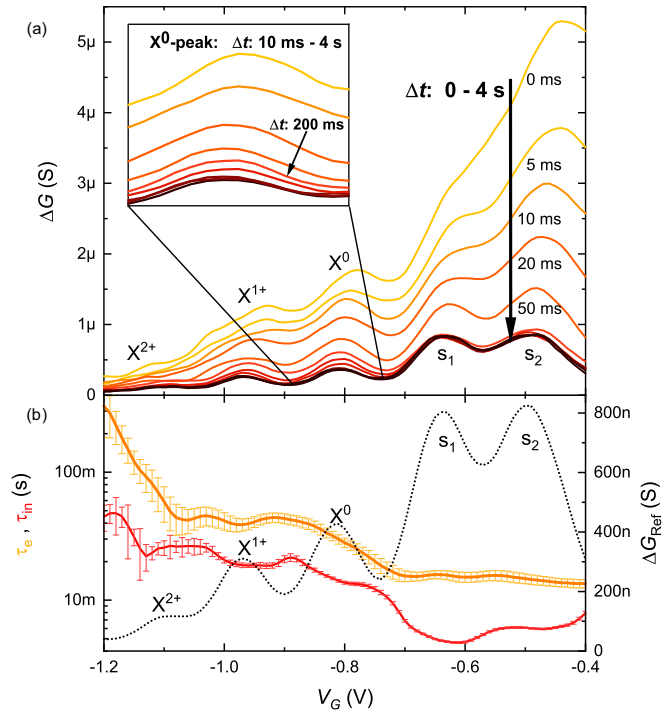

FIG. 8. (a) Charging spectra with increasing settling time Δt from 0 to 4 s after the illumination pulse ended. The huge peaks originate from an overlap of the charging pulse with the depopulation of the nonequilibrium light-induced states for short Δt. The inset shows the scaled-up X^0 peak and its partial decay into a metastable steady state. (b) Time constant τ_{e} (orange) for the initial decline of the charging spectra into metastable equilibrium from (a) calculated with exponential fits at given gate voltages. For qualitative comparison, τ_{in} (red) is taken from the equilibrium tunneling as it is already shown in Fig. 3(c).

Therefore Fig. 6(a) shows the conductance response G_{illu} to the 200 ms LED illumination cut out of the full sequence with the light pulse active in between $t = 0$ ms and $t = 200$ ms for different gate voltages. The three additional sketches depict the valence and conduction band around the QD and 2DEG for $V_{\mathrm{G}} = -1.10$ V [Figs. 6(b) and 6(c), excitonic range] and -0.50 V [Fig. 6(d), s_2 peak] as well as the participating charge carriers. The arrows indicate the electron-hole excitation (black dashed), electron tunneling (blue), and electron-hole recombination (orange) responsible for the corresponding behavior in Fig. 6(a).

The conductance of the channel is proportional to mobility and carrier concentration. As shown by Kurzmann *et al.*, a rise in conductance correlates with an increased amount of electrons inside the 2DEG channel and vice versa [16], whereas the influence due to Coulomb scattering of charged QDs is negligible [17]. Taking that into account, the light-induced rise and fall in the 2DEG conductance is a directly related to the temporal charge state of the QDs.

To evaluate the response of the 2DEG channel to the illumination, Fig. 7(a) shows the absolute conductance increase at the beginning (red plot) and decrease at the end of the light pulse (blue plot).

We find a broad huge peak in the excitonic regime for the red curve, as well as a huge peak after the s_2 and another increase after the p_4 peak. For $V_{\mathrm{G}} > -0.7$ V, the red and the blue curve are on top of each other. Furthermore, dip features occur on both curves in the bias range of the s_1 and p_1 charging state. The blue curve has peaks and dips in the excitonic bias range that are inverse to the ones at the equilibrium spectra.

As an extension to the absolute change due to illumination in Fig. 7(a), Fig. 7(b) shows the time-resolved differential evolution of the conductance. The resulting $\Delta G(t)$ is transformed into an average amount of light-induced charges ΔQ_{i} per QD calculated by nonequilibrium ΔG measurements (see Fig. 9 in the Appendix). What we observe is a fundamentally different response for two regions: A partial decay for $V_{\mathrm{G}} < -0.7$ V and otherwise a complete decay in the differential conductance.

We now interpret the findings of Figs. 6 and 7. Due to the reset pulse, QDs reside in equilibrium without any metastable holes left over at the beginning of each measurement cycle. During the illumination, QDs are brought into a dramatic nonequilibrium state, since they are up to sixfold more positively charged than in equilibrium. While the light-induced electron-hole generation rate is constant,

this temporal nonequilibrium only depends on V_G via the corresponding tunnel coupling to the 2DEG channel. On charge state resonances, the tunnel coupling is strong and the electron tunneling in dominates the light-induced electron-hole generation. As a result, dips in the conductance change occur. In contrast, peaks occur in regions where electron tunneling is not resonant. Thus, positive charges pile up until a level where electron tunneling in is efficient again.

The red curve depicts the absolute conductance increase during illumination and represents accumulated light-induced metastable holes for $V_G < -0.7$ V. For higher gate voltages ($V_G > -0.7$ V) with charge states in resonance to the 2DEG, it corresponds to missing electrons (light-induced holes annihilate the already charged QDs) plus additional nonequilibrium holes. The blue curve in the same graph is taken from the absolute conductance decrease when the illumination ends. For $V_G > -0.7$ V it is aligned with the red curve, indicating that all light-induced nonequilibrium states (missing electrons plus nonequilibrium holes) that build up during the illumination are annihilated up to the Fermi energy, while the QDs are recharged by tunneling electrons from the 2DEG channel.

Figure 7(b) shows the temporal evolution of the metastable and nonequilibrium state creation and annihilation processes. After the illumination ends, one can observe the storage of metastable hole states for $V_G < -0.7$ V and fast depopulation of surplus holes and refilling of the missing electrons for higher gate voltages.

We now discuss three mechanisms that could eliminate those light-induced hole states. The first and major process are direct tunneling electrons from the 2DEG. The previous results made clear that for gate voltages above the first QD charging state ($V_G > -0.7$ V) all holes are rapidly depopulated by this after the illumination stopped.

For the excitonic bias range, metastable stored holes remain inside the QDs up to the according gate voltage. Those may get lost over time either by spontaneous direct recombination with electrons from the 2DEG where tunneling in can occur resonantly into many-particle states, or via spatial indirect transition of a hole into the SPS barrier and drifting to the gate [18].

To get a glimpse of the actual storage time of these holes in our device, we now reintroduce the charging pulse V_C upon variation of the time delay Δt (settling time in Fig. 2) after the light pulse ended. The resulting ΔG of the charging pulse transient after that delay is plotted in Fig. 8(a). One can observe a fast initial peak decline into metastable equilibrium for small Δt and its decay is calculated with exponential fits. The resulting τ_e is plotted over V_G in Fig. 8(b) as well as τ_{in} taken from the equilibrium tunneling for the purpose of peak position comparison.

What we observe is a quick initial decay in the time range of $\Delta t < 100$ ms for $V_G > -0.7$ V. The excitonic peaks seem stabilized after $\Delta t \approx 500$ ms and we propose that up to 4 s and probably beyond, metastable stored holes for $V_G < -0.7$ V remain inside the QDs since we see no further peak decay.

The explanation for the increased peak height for short Δt in Fig. 8(a) is directly based on the previous results for the illumination pulse dynamic. On that time scale, the charging pulse overlaps with the depopulation of the surplus holes and missing electrons directly after the illumination.

The final part is addressed to the quantitative analysis of the depopulation dynamic represented by τ_e in Fig. 8(b). The nonmonotonous behavior indicates that the decreasing peaks are not likely to be dependant on *DX* centers, but the tunnel and memory dynamics of the QDs. There is a qualitative agreement to the equilibrium tunneling dynamic τ_{in} but a slower decay due to the larger number of consecutive tunneling electrons during the depopulation process. The series process has resonant and nonresonant tunneling contributions resulting in relatively long relaxation times. We observe a qualitative disagreement however in the *s*-peak bias range where no spin degeneracy features exist for τ_e. Valentin *et al.* showed that nonequilibrium *p*-state tunneling takes place in this bias range [19].

According to these studies, nonequilibrium states like X^{0*} (X^{1+*}) as they call it consisting of one (two) hole(s) and one electron tunneling into a *p* state take place at gate voltages slightly higher than the s_1 (s_2) resonances. These new channels explain the right-shifted peaks as well as the peak broadening as it can be observed for $\Delta t < 100$ ms in Fig. 8(a). Due to the high amount of nonequilibrium hole states in this bias range, we thus conclude that a multiplet of additional transitions into different levels and charge states must exist. Those could be tunneling into *d* or even *f* states while

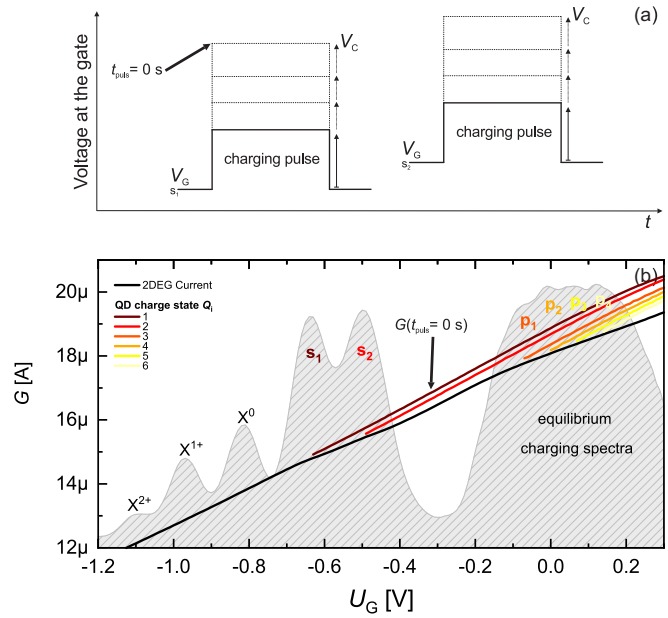

FIG. 9. (a) Sketch of the gate pulse sequence that was used to separate the change in conductance due to an increased gate voltage (normal field effect transistor) from the influence of the QD charging. V_G is set to a peak voltage (e.g., s_1 $V_G = -0.64$ V) and the added charging pulse voltage is successively increased. This is done for different V_G at each peak and the conductance $G(t_{puls} = 0\text{ s})$ is taken at the beginning of each pulse transient. At that point, the QD remain in the charging situation given by the bias voltage while the much faster 2DEG conductance already reacted to the increased voltage. (b) The resulting $G(t_{puls} = 0\text{ s})$ for every charging peak and the conductance change caused by the increasing gate voltage (black base line). The actual QD charge state Q_i is taken from the conductance difference between each line at the corresponding charging peak voltages.

Coulomb attraction from more holes pulls these states into the according gate voltage range. The various configurations then broaden these higher-level contributions and are thus not clearly resolved as also observed by Marquardt *et al.* [8].

IV. CONCLUSIONS AND OUTLOOK

By near-infrared illumination of a 2DEG-QD structure, the temporal evolution of electrons tunneling into quasiequilibrium states was shown up to X^{2+}. Hole storage times of at least 4 s after an initial equilibration process of about 500 ms were found. In contrast to previous works with longer storage times [20,21], the hole creation process in this work is optically induced and thus in principle suitable for a fast optical write and electronical read and erase memory of single charge quanta. Furthermore, as the erase mechanism creates single photons from the exciton recombination, the device promises the creation of flying qubits. By adapting the tunnel barrier, the device could either be optimized for higher hole storage times or for a shorter time to reach equilibrium after the illumination. Anyway, this flexibility is a huge advantage of such a nonequilibrium light-induced hole memory. Our experiments can be further expanded to nonequilibrium tunnel processes [8,19] and quantum dot molecules.

ACKNOWLEDGMENTS

For financial support the authors thank the BMBF via the QuaHL-Rep, Contracts No. 16BQ1034 and No. 16BQ1035. We would like to thank N. Viteritti for expert sample preparation.

APPENDIX: ADDITIONAL FIGURES

Figure 9(a) presents the basic measurement principle used to separate the influence on the 2DEG conductance ΔG due to an increased gate voltage V_G and by the transfer of electrons into the QDs. The results in Fig. 9(b) are used to determine the actual QD charge state Q_i as it is used for the time-resolved differential evolution of the 2DEG during the illumination in Fig. 7(a).

[1] M. Stubenrauch, G. Stracke, D. Arsenijević, A. Strittmatter, and D. Bimberg, Appl. Phys. Lett. **105**, 011103 (2014).
[2] A. Marent, T. Nowozin, M. Geller, and D. Bimberg, Semicond. Sci. Technol. **26**, 014026 (2010).
[3] M. Ediger, G. Bester, A. Badolato, P. M. Petroff, K. Karrai, A. Zunger, and R. J. Warburton, Nat. Phys. **3**, 774 (2007).
[4] A. V. Kuhlmann, J. Houel, D. Brunner, A. Ludwig, D. Reuter, A. D. Wieck, and R. J. Warburton, Rev. Sci. Instrum. **84**, 073905 (2013).
[5] A. V. Kuhlmann, J. H. Prechtel, J. Houel, A. Ludwig, D. Reuter, A. D. Wieck, and R. J. Warburton, Nat. Commun. **6**, 8204 (2015).
[6] P. A. Labud, A. Ludwig, A. D. Wieck, G. Bester, and D. Reuter, Phys. Rev. Lett. **112**, 046803 (2014).
[7] B. Marquardt, M. Geller, A. Lorke, D. Reuter, and A. D. Wieck, Appl. Phys. Lett. **95**, 022113 (2009).
[8] B. Marquardt, M. Geller, B. Baxevanis, D. Pfannkuche, A. D. Wieck, D. Reuter, and A. Lorke, Nat. Commun. **2**, 209 (2011).
[9] J. Houel, A. V. Kuhlmann, L. Greuter, F. Xue, M. Poggio, B. D. Gerardot, P. A. Dalgarno, A. Badolato, P. M. Petroff, A. Ludwig, D. Reuter, A. D. Wieck, and R. J. Warburton, Phys. Rev. Lett. **108**, 107401 (2012).
[10] A. Beckel, A. Kurzmann, M. Geller, A. Ludwig, A. D. Wieck, J. König, and A. Lorke, Europhys. Lett. **106**, 47002 (2014).
[11] H. Drexler, D. Leonard, W. Hansen, J. P. Kotthaus, and P. M. Petroff, Phys. Rev. Lett. **73**, 2252 (1994).
[12] R. J. Warburton, B. T. Miller, C. S. Dürr, C. Bödefeld, K. Karrai, J. P. Kotthaus, G. Medeiros-Ribeiro, P. M. Petroff, and S. Huant, Phys. Rev. B **58**, 16221 (1998).
[13] D. V. Lang, R. A. Logan, and M. Jaros, Phys. Rev. B **19**, 1015 (1979).
[14] P. M. Mooney, J. Appl. Phys. **67**, R1 (1990).
[15] W. Lei, M. Offer, A. Lorke, C. Notthoff, C. Meier, O. Wibbelhoff, and A. D. Wieck, Appl. Phys. Lett. **92**, 193111 (2008).
[16] A. Kurzmann, B. Merkel, B. Marquardt, A. Beckel, A. Ludwig, A. D. Wieck, A. Lorke, and M. Geller, Phys. Status Solidi B **254**, 1600625 (2017).
[17] A. Kurzmann, A. Beckel, A. Ludwig, A. D. Wieck, A. Lorke, and M. Geller, J. Appl. Phys. **117**, 054305 (2015).
[18] A. K. Rai, S. Gordon, A. Ludwig, A. D. Wieck, A. Zrenner, and D. Reuter, Phys. Status Solidi B **253**, 437 (2015).
[19] S. R. Valentin, J. Schwinger, P. Eickelmann, P. A. Labud, A. D. Wieck, B. Sothmann, and A. Ludwig, Phys. Rev. B **97**, 045416 (2018).
[20] L. Bonato, E. M. Sala, G. Stracke, T. Nowozin, A. Strittmatter, M. N. Ajour, K. Daqrouq, and D. Bimberg, Appl. Phys. Lett. **106**, 042102 (2015).
[21] M. Geller, A. Marent, E. Stock, D. Bimberg, V. I. Zubkov, I. S. Shulgunova, and A. V. Solomonov, Appl. Phys. Lett. **89**, 232105 (2006).